Article

Production and Characterization of Bioactive and Antimicrobial Titanium Oxide Surfaces with Silver Nanoparticles and a Poly(lactic acid) Microfiber Coating

Karina M. Zaniolo,[a] Sonia R. Biaggio,[a] Joni A. Cirelli,*,[b] Mariana A. Cominotte,[b] Nerilso Bocchi,[a] Romeu C. Rocha-Filho [iD] *,[a] and Clovis W. O. de Souza[c]

[a]*Departamento de Química, Universidade Federal de São Carlos (UFSCar), 13565-905 São Carlos-SP, Brazil*

[b]*Departamento de Diagnóstico e Cirurgia, Faculdade de Odontologia, Universidade Estadual Paulista (Unesp), 14801-903 Araraquara-SP, Brazil*

[c]*Departamento de Morfologia e Patologia, Universidade Federal de São Carlos (UFSCar), 13565-905 São Carlos-SP, Brazil*

Silver nanoparticles (AgNp) were deposited on highly porous TiO$_2$ surfaces by the dripping of a colloidal AgNp solution to provide antimicrobial activity. Micro-porous TiO$_2$ surfaces were obtained on commercially pure titanium by micro-arc oxidation in an electrolyte containing Ca and P precursors. In addition, as silver can be toxic to cells, these surfaces were uniformly covered with the biocompatible and bioresorbable poly(lactic acid) (PLA) polymer by electrospinning, aiming at promoting a controlled release of silver ions to the medium. The resulting AgNp-containing surfaces were characterized by scanning electron microscopy (SEM), energy dispersive spectrometry (EDS) and X-ray diffraction (XRD), and *in vitro* assays were performed to evaluate their antimicrobial activity and bioactivity. Tests revealed that the surfaces showed antimicrobial activity against *Staphylococcus aureus*, with better results for the surfaces without PLA. However, all the surfaces presented good biocompatibility in assays with mouse MC3T3-E1 pre-osteoblasts, and greater cell differentiation for the polymer-coated surfaces. Finally, the PLA ultrafine fibers electrospun on the TiO$_2$/AgNp surfaces allowed a controlled release of silver ions in the phosphate-buffered saline (PBS) medium.

Keywords: bioactive porous TiO$_2$ surface, antimicrobial TiO$_2$ coating, silver nanoparticles, poly(lactic acid) coating, silver-ions release

Introduction

Even after years of scientific studies, the success rate of dental implants is still just over 90%. Usually, when a failure occurs, the implant is removed and before inserting a new device, healing and probable local bone filling must first occur, which takes months.[1] One of the main causes of implant failure is aseptic loosening.[2] This complication usually happens when complete osseointegration does not occur between the peri-implant bone and the implant surface. Another cause of implant failure is bacterial infection, which can lead to serious health problems and significantly reduces the quality of life of the patients. In severe cases, the spread of infection occurs, leading to

patient death.[1,3] Therefore, research strategies for surface modification aiming at reducing bacterial infections are welcome.

To be successfully used, an implant must have adequate mechanical properties such as elasticity, ductility, hardness, fatigue and wear resistance, and good biocompatibility. Therefore, titanium (Ti) and its alloys are the first choice materials due to some of their properties when compared to other metallic materials: high corrosion resistance, low density and low modulus of elasticity, as well as excellent biocompatibility.[4,5]

The topography and composition of implants play a decisive role in their performance by modulating the surface interaction with cells and microorganisms, preventing aseptic loosening.[1] Shalabi *et al.*[6] reported that rougher Ti surfaces show better proliferation and adhesion of osteoblasts, and improve alkaline phosphatase response and

*e-mail: romeu@ufscar.br; joni.cirelli@unesp.br

bone mineralization when compared to smoother surfaces. It is believed that roughness promotes interconnection between cells at the micrometer scale. Furthermore, not only microtopography but also nanotopography is important for this process.[3,7]

The chemical composition of the implant surface is also critical in the osseointegration process. When elements such as calcium and phosphorus are present in the surface, there is an increase in protein adsorption that leads to an early biological fixation of the implant.[7] Besides Ca and P, other elements such as Sr, Se and Si can also improve the surface biocompatibility.[8,9]

Several techniques and treatments may be used to modify an implant surface to improve its osseointegration and reduce the risk of infections: 3D printing, laser surface texturing, micromachining, mechanical polishing, sandblasting, ion implantation, chemical etching and several coating techniques, such as chemical or physical vapor deposition, plasma spraying, thermal oxidation, and anodization.[7,10,11] Among them, anodization has stood out as it allows, through proper adjustment of the experimental parameters, greater control of the thickness, composition, morphology and structure of the formed oxide layer.[12] Furthermore, several studies[13,14] have reported that corrosion resistance and osseointegration are improved when anodized cp Ti (commercially pure titanium) is used.

Seeking to prevent infection when inserting an implant, patients are routinely medicated with high doses of antibiotics intravenously and/or orally.[15] However, pharmacological treatments have limitations, regardless of their administration route; among them, low drug solubility, poor distribution in the body, lack of selectivity, uncontrolled pharmacokinetics and serious adverse effects in non-target tissues may occur.[16] In addition, such treatments are often ineffective due to poor vascularization in the vicinity of the implanted device.[17] The use of locally controlled drug release with polymers has successfully circumvented some of these problems. Nevertheless, despite the effectiveness of this method, it is still restricted by the sensitivity of bacterial species to the supplied antibiotic.[18] In addition, due to the indiscriminate use of antibiotics, whether for therapeutic action or other purposes, many resistant bacteria have emerged. This has become a major public health problem, making essential the search for alternatives to antibiotics.[19,20]

The use of elements such as Zn, Cu, Ga and Ag in Ti implants has been successfully tested as antimicrobial agent alternatives to antibiotics.[8,9] Among them, silver, especially in nanoparticulate form (AgNp), is promising as it reaches a wide range of bacteria.[19,21,22] In their 2018 review, Mi *et al.*[8] point out that the use of metal, metal oxide, and solid lipid nanoparticles was being increasingly explored as an alternative for the routine treatment of infections. These nanoparticulate materials can be used both as antimicrobials themselves or in conjunction with antibiotics to potentiate their effect. The chemical synthesis method of AgNp stands out for its versatility, low cost, and ability to produce particles with well-defined morphology, size and structure.[23] In recent years, its biological synthesis has called attention mainly because it is considered eco-friendly, but the control of the AgNp basic parameters is still not very accurate.[24] Considering that size, purity and morphology play a crucial role on the AgNp antimicrobial response, the chemical synthesis method was chosen in the present work due to its best performance to produce nanoparticles with the desired properties.

Several studies on the anodization of Ti and its alloys by micro-arc oxidation (MAO) were carried out in electrolytes containing precursors of P, Ca and Ag.[25,26] Although the resulting materials showed good antimicrobial response to *Staphylococcus aureus*, Ag was incorporated mostly into the Ti oxide layer and, therefore, did not contribute to the achieved result. Another approach was AgNp deposition after MAO anodization, thus making accessible all the deposited Ag; in fact, the antimicrobial activity of these materials was excellent against some types of bacteria: *S. aureus*, *S. aureus* resistant to methicillin, *Staphylococcus epidermidis*, and *Escherichia coli*.[27,28]

A concern about using silver as an antimicrobial agent is that, depending on its concentration, it can be toxic to humans. However, some authors[29,30] suggest that the toxicity of silver is reduced when used in the nanoparticulate form compared to that in the ionic form, since the AgNp ion release mechanism is much slower because silver is only partially oxidized. In addition to being an excellent antimicrobial agent, it has been reported that in non-toxic concentrations AgNp has properties that enhance osteoinduction and regulate the proliferation and differentiation of mesenchymal stem cells that act in bone regeneration.[31]

To minimize the toxicity of silver on titanium surfaces, a polymeric coating can also be used. Depending on the polymer, other characteristics can be added to the material, for example, greater biocompatibility or control of silver release to the medium. A wide range of natural or synthetic polymers can be used for this purpose.[32] However, natural polymers generally have drawbacks such as high costs, low reproducibility, and questionable purity. On the other hand, synthetic polymers do not present such problems; among them, poly(lactic acid) (PLA) has been widely used because it is easily produced, being a low-cost, commercially available polymer of biological basis. Moreover, as PLA is biodegradable, biocompatible, bioresorbable, compostable,

2 of 14

J. Braz. Chem. Soc. **2024**, *35*, 3, e-20230134

non-toxic, and presenting some desirable mechanical properties, it is considered the most promising substitute for petroleum-derived polymers.[33]

Various polymer coating methods may be used for this process,[34,35] but electrospinning has been increasingly applied due to its simplicity and versatility. Because of properties such as their high surface area/volume ratio and porosity, nanofibers produced by electrospinning have been considered for application in filtration systems, chemical and optical sensors, tissue engineering, wound healing, energy storage, enzyme carrying, and drug delivery.[36] The use of electrospinning to produce PLA nanofibers with or without additives has been promising in biomedical applications.[37,38] Chen *et al.*[39] developed nanofiber scaffolds for cartilage regeneration produced by electrospinning a PLA and gelatin solution. These devices showed excellent cytocompatibility and high resorption rates.

Considering the above, the aim of this work was to deposit AgNp on a highly porous titanium oxide to obtain an efficient antimicrobial and bioactive surface, as well as to coat this surface with PLA to minimize the AgNp toxicity and to attain a controlled release of silver ions in the biological medium. To achieve this, a porous TiO_2 surface was first obtained by MAO, followed by the AgNp deposition; then, this modified surface was coated with PLA by electrospinning. Finally, the modified Ti surfaces (Ti/TiO_2/AgNp, Ti/TiO_2/PLA and Ti/TiO_2/AgNp/PLA) were physically characterized and submitted to biocompatibility and antibacterial tests.

Experimental

Synthesis of silver nanoparticles (AgNp)

AgNp was synthesized by the sodium borohydride ($NaBH_4$, Sigma-Aldrich, St. Louis, USA) reduction method. Silver nitrate ($AgNO_3$, Sigma-Aldrich, St. Louis, USA) was used as the Ag precursor and sodium citrate ($Na_3C_6H_5O_7$, Sigma-Aldrich, St. Louis, USA) as a stabilizing agent. The concentrations and volumes of the solutions of these reagents are shown in Table 1.

First, 100 mL of the $Na_3C_6H_5O_7$ solution and 1.0 mL of the $AgNO_3$ solution were placed in a 250 mL reaction vessel

Table 1. Volume and concentration of solutions used in the AgNp synthesis

Reagent	Concentration / (10^{-2} mol L^{-1})	Volume / mL
$Na_3C_6H_5O_7$	0.05	100
$AgNO_3$	2.5	1.0
$NaBH_4$	11	1.0

and kept under constant magnetic stirring, at approximately 0 °C. Then, 1.0 mL of the $NaBH_4$ solution was dripped on that resulting solution at a flow rate of 0.5 mL *per* min, using a syringe pump (KD Scientific, model KDS 100, Holliston, USA). Subsequently, the thus obtained colloidal silver solution was stored at room temperature in the absence of light.

Characterization of silver nanoparticles (AgNp)

The UV-Vis spectra of the colloidal silver solutions were obtained in a spectrophotometer (Jasco V-660), at room temperature, in the wavelength region of 300-800 nm, using quartz cuvettes with 1 cm of optical path and distilled water as standard.

X-ray diffraction (XRD) analyses to characterize the AgNp crystalline structure were performed using a Shimadzu diffractometer (model XRD 6000), with a Cu Kα radiation source (λ = 1.54056 Å), a voltage of 30 kV and a current of 30 mA. Measurements were made in the continuous-scanning mode in the range $35° \leq 2\theta \leq 85°$, at a scanning rate of 0.2° min^{-1}. The AgNp solution was dripped on a silicon substrate. The identification of the AgNp crystalline phases was performed using diffractograms obtained from tabulated patterns available in the Joint Committee on Powder Diffraction Standards-Powder Diffraction File (JCPDS-PDF) database.

Dynamic light scattering (DLS) analysis was performed to determine the size of the particles in solution, at room temperature (ca. 25 °C), using a Zetasizer Nano ZS system (Malvern Instruments, Malvern, UK). Zeta potential measurements were performed with the same equipment to determine the AgNp surface potential and its stability at different pH values in the range of 2.2-11.2. These pH values were adjusted with the aid of an MPT-2 multi-purpose titrator (Malvern Instruments, Malvern, UK), using 0.01 mol L^{-1} HNO_3 and 0.01 mol L^{-1} NaOH solutions. Measurements were performed in triplicate.

To analyze the AgNp particle size, morphology and nanostructure, transmission electron microscopy (TEM) images were obtained using a TECNAI F20 microscope, operating at 200 kV. Measurements in the high-resolution mode were also performed. Prior to obtaining the images, a drop of the aqueous AgNp suspension was placed on a carbon-coated copper grid and dried in air.

Preparation of the silver-deposited TiO_2 coatings

A commercially pure titanium (Ti cp) plate (purity > 99% in mass) was acquired from Titanews (Barueri, Brazil). Titanium disks (diameter (Φ) = 12.6 mm, thickness (*h*) = 2 mm)

J. Braz. Chem. Soc. **2024**, *35*, 3, e-20230134

3 of 14

were used to prepare micro and nanoporous surfaces of TiO_2, as previously described.[10] Briefly, MAO treatment was performed to anodize the titanium samples at room temperature (about 23 °C), using a DC power supply (Tectrol, Londrina, Brazil) at 250 V for 1 min, under magnetic stirring. The aqueous electrolyte solution was a mixture of 0.167 mol L^{-1} calcium acetate hydrate ($Ca(CH_3COO)_2.H_2O$) and 0.100 mol L^{-1} potassium phosphate (K_3PO_4).

Silver nanoparticles were deposited on the anodized Ti surfaces. For that, 3.0, 5.0, 10.0 and 15.0 mL of the AgNp solution were dripped on the anodized Ti surface with the aid of a pipettor. While dripping, the surfaces were kept on a heating plate maintained at 250 °C.

Polymeric coating with PLA fibers by electrospinning

The polymeric solutions used in the process of obtaining the PLA fibers were prepared by dissolving poly(lactic acid) (66,000 g mol^{-1}, Nature Works, Minneapolis, USA) in chloroform and dimethylformamide (DMF) (3:1 v/v), defining a final PLA concentration of 10 or 14% m/m. First, PLA was added to chloroform under constant magnetic stirring, at room temperature, until complete polymer dissolution. Then, DMF was added to promote charges in the polymeric solution that are essential for the electrospinning process.

The experimental configuration of the electrospinning setup consisted of a high voltage direct current power supply (Spellman SL series), a collector, a syringe pump (model KDS 100, from KD Scientific, Holliston, USA) and a syringe oriented with the needle perpendicular to the collector. The collector consisted of a metal cylinder covered with an aluminum foil where the samples were fixed. A high voltage was applied between the collector and the syringe needle. The polymer solution loaded into a syringe was extruded from the tip of the needle by the syringe pump at a constant flow rate. At the ejection point (the tip of the needle), a jet of polymer is formed because of the repulsion of electrical charge that comes out of the surface tension of the solution. The electrospinning parameters were adjusted as flow rate: 1.2 mL h^{-1}, voltage: 22.2 kV, distance from the needle tip collector: 9 cm, needle diameter: 1.2 mm, spinning time: 2, 3, 4, 5, 10 and 15 min, and collector rotation rate: 400 rpm. The electrospinning was carried out at 25 °C and 40% relative humidity in a closed acrylic box.

Physical characterization of the coatings

The surface morphology and composition of the Ti/TiO$_2$/AgNp and Ti/TiO$_2$/PLA samples were investigated by scanning electron microscopy (SEM) using a Philips XL-30 FEG microscope, Eindhoven, Netherlands; the Ti/TiO$_2$/AgNp sample was also investigated by energy dispersive spectrometry (EDS). In addition, the crystalline structure of the TiO$_2$/AgNp surface was analyzed by XRD also using the Shimadzu model XRD 6000 diffractometer. Measurements were made in the continuous-scanning mode in the range $20° \leq 2\theta \leq 80°$, at a scanning rate of 2° min^{-1} with a scan step of 0.02°.

Biological tests

In vitro tests were used to analyze the biocompatibility of the modified Ti surfaces (Ti/TiO$_2$; Ti/TiO$_2$/PLA; Ti/TiO$_2$/AgNp and Ti/TiO$_2$/AgNp/PLA), providing data to evaluate cell morphology, adhesion, differentiation, and proliferation of murine pre-osteoblasts MC3T3-E1 cells (BCJR, Brazil). More details about the used protocol are available in a previous work.[10]

Cell culture and seeding

Pre-osteoblasts cells were cultured in an alpha-minimum essential medium (αMEM, Gibco, Thermo Fisher Scientific, Waltham, USA) supplemented with 10% fetal bovine serum (FBS, Gibco), 100 U mL^{-1} penicillin (Gibco) and 100 µg mL^{-1} streptomycin (Gibco) in a humidified atmosphere of 5% CO$_2$ at 37 °C. The medium was refreshed every 3 days until the cells reached 80-90% confluency. Then, the cells were detached with a trypsin-ethylenediaminetetraacetic acid (EDTA) solution (Gibco) and seeded on the samples (previously sterilized with gamma radiation) at a density of 2×10^4 cells mL^{-1}. Here, 50 µg mL^{-1} ascorbic acid (Sigma-Aldrich, St. Louis, USA) and 10 mmol L^{-1} β-glycerophosphate (Sigma-Aldrich, St. Louis, USA) solutions were added to the culture medium.

Cell viability evaluation

Cell viability was evaluated after 24, 48 and 72 h using the alamarBlue® kit (Life Technologies, Carlsbad, USA). Cells were cultured on the samples and placed in a 24-well plate. After the experimental time points, the adhered cell was incubated for 4 h, at 37 °C, with 500 µL of working solution: α-MEM with 10% FBS, 1% P/S (penicillin/streptomycin) and 10% alamarBlue®. Wells without samples, having only the working solution, were used as blank controls. Subsequently, the optical density (OD) was measured at 570 and 600 nm on a microplate reader. The samples were the same in all periods of the experiment. The supernatant was collected for reading, and then washed

once with the phosphate-buffered saline (PBS) solution; then, a fresh culture medium was inserted, repeating this procedure until the last period.

Cell morphology

The cell spreading, proliferation and morphology on the samples were evaluated by direct fluorescence microscopy after 1, 3 and 7 days of culture. For the immunofluorescence analyses, phalloidin conjugated with the Alexa Fluor® 488 dye (Molecular Probes, Eugene, USA) was used to signal the actin cytoskeleton, whereas 4,6-diamidino-2-phenylindole dihydrochloride (DAPI, Molecular Probes) was used for nuclear labeling. Acquisition of the cell images was performed in an inverted fluorescence microscope (Evos FL, AMG Micro, Bothell, USA).

Mineralized nodule formation

To analyze the mineralization process, the extracellular matrix (ECM) mineralization produced by the osteoblast-like cells on the samples after culturing for 21 days was stained with alizarin red. Briefly, the samples were rinsed twice with the PBS solution at 37 °C, fixed with 70% (v/v) ethanol at 4 °C for 1 h, rinsed twice with deionized water and stained with an alizarin red solution (40 mmol L^{-1}, pH 4.2, Sigma-Aldrich, St. Louis, USA) under gentle shaking (VDRL Shaker, Biomixer), at room temperature, for 5 min, in the dark. Before taking pictures, the excess non-adherent dye was washed off by copiously washing the samples with deionized water. For the alizarin red quantification, the dye was dissolved with a 10% cetylpyridinium chloride solution (Sigma-Aldrich, St. Louis, USA) under stirring for 15 min, at room temperature. To measure the absorbance at 550 nm, 100 μL aliquots were read in a microplate reader (Power Wave XS, BioTek Instruments, USA). Three measurements were performed for each sample.

Antibacterial tests: bacteria culture (inoculum preparation)

Antimicrobial activity tests were performed to assess the sensitivity of *Staphylococcus aureus* on different Ti surfaces. First, the samples were sterilized by exposure to UV radiation for 15 min on each side. Anodized titanium disks (Ti/TiO$_2$ samples) were used as a negative control. To prepare the inoculum, the bacterial strain *S. aureus* (ATCC 25923) was previously activated by transferring from the stock culture (−20 °C) to a Müller Hinton (MH) pH 7.3 ± 0.1 (Oxoid®, Thermo Fisher Scientific, Waltham, USA) medium and incubated for 24 h at (36 ± 1) °C. Afterwards, the culture was centrifuged

for 10 min at 3600 rpm, the supernatant was discarded, and the pellet was resuspended in the PBS solution. To standardize the inoculum in the disc diffusion tests, absorption measurements were performed at 600 nm in a spectrophotometer (Femto, model 600) to obtain a concentration of approximately 10^8 colony forming units *per* milliliter (CFU mL^{-1}). For antibacterial activity tests using a methodology adapted from the Japanese Industrial Standard,[40] the suspensions were diluted to obtain an initial inoculum of 10^6 CFU mL^{-1}.

Antibacterial tests: disc diffusion

The disk diffusion tests were adapted from the Standard M2-A8, adopted by ANVISA with permission of CLSI (Clinical and Laboratory Standards Institute).[41] The formation of the inhibition zones depends on the antimicrobial agent diffusion and the solubility in the MH agar. Therefore, the inoculants were first spread with a sterile swab on plates containing the MH medium. Afterwards, the modified and control samples (n = 3) were placed on the MH agar with the treated surface facing downwards and immediately incubated at (36 ± 1) °C for 24 h. Finally, photographs of the plates were taken and the inhibition zones were measured. All measurements were performed in triplicates.

Antibacterial activity assays

The antibacterial activity assays were conducted using an adapted methodology proposed by the Japanese Industrial Standard (JIS) Z 2801:2010.[40] Briefly, after sterilization, the samples were placed in the wells of a 24-well plate, which, after addition of 30 μL of the *S. aureus* bacterial inoculum (forming a suspension thin layer in direct contact with the specimens), were covered with a previously sterilized polyethylene film.

The plates were incubated at (36 ± 1) °C for 24 h in a humid chamber. After, the samples were carefully transferred to 15 mL Falcon tubes containing 1 mL of the PBS solution, previously sterilized. Then, serial dilutions were performed 10 to 100,000 times using the PBS solution. The spread plate method was used for the quantitative evaluation of cells, in which 25 μL of all dilutions and the original suspension were spread, with the aid of sterile Drigalsky loops, in duplicate plates containing the plaque counting agar (PCA) culture medium (pH 7.3 ± 0.1, Oxoid®). These plates were incubated at (36 ± 1) °C for 24 h and then the CFU was counted. Additionally, to evaluate the solution without dilution, the rest of the suspension (850 μL) was inoculated using the pour plate method in

J. Braz. Chem. Soc. **2024**, *35*, 3, e-20230134

5 of 14

the PCA culture medium. The plates were incubated at (36 ± 1) °C for 48 h and then the CFU was counted.

Quantification of silver-ion release

To investigate the release behavior of Ag^+ ions from $Ti/TiO_2/Ag$ and $Ti/TiO_2/Ag/PLA$, the samples (n = 3) were immersed in 5 mL of the PBS solution (pH 7.4) for 43 days, under static conditions at 37 °C in the absence of light. Then, the PBS solution was refreshed at predetermined time intervals (daily for the first 15 days and subsequently only on days 22, 29, 36 and 43). The concentration of released Ag^+ ions was determined using inductively coupled plasma optical emission spectrometry (ICP-OES, model iCAP 7000, Thermo Fisher Scientific, Waltham, USA). Additionally, after the last collection period, the remaining Ag^+ ions were extracted with 10 mL of a 30% HNO_3 solution and then quantified.

Statistical analysis

Significant statistical differences between groups were evaluated for all the quantitative data and presented as mean ± standard deviations. One-way analysis of variance (ANOVA) was used to determine the significant difference in the results obtained by the biological and antibacterial tests. However, the cell viability and the mineralized nodule formation assays were followed by the Tukey's post hoc test. The significance level was set at 5% ($p < 0.05$).

Results and Discussion

Characterization of the synthetized AgNp

A photo of the final solution remaining from the Ag nanoparticle synthesis is shown in Figure 1a; the yellow aspect is characteristic of AgNp colloidal solutions due to surface plasmon resonance. For spherical silver nanoparticles, generally in the 2-100 nm range, the reported maximum absorption wavelength is around 400 nm.[28,42,43] In this work, the maximum absorption occurred around 390 nm (see Figure 1c).

The obtained AgNp was deposited on a silicon substrate for crystal structure analysis by XRD. The peaks observed in the diffractogram shown in Figure 1b correspond to Ag with cubic structure, according to the crystallographic card JCPDS-PDF No. 4-783. For further characterization, one silver nanoparticle was isolated with the aid of the TEM technique. From the measurement of the distances between the crystalline planes, highlighted in yellow in Figure 1b, it

was possible to index the (111) plane of the metallic silver to a face-cubic centered (FCC) arrangement.

To assess the synthesis reproducibility, the AgNp solution was prepared in six replicates. First, as can be seen in Figure 1c, there was no wavelength shift of the plasmonic band maximum absorption over time. Additional tests were also performed to evaluate the stability of the AgNp solution over time at different pH values. As can be seen in Figure 1d, there was no decrease in the maximum average absorbance intensity even after 30 days of the AgNp solution synthesis.

To analyze the AgNp solution stability as a function of pH, zeta potential measurements were performed. These measurements can be used to determine the surface charge of a particle dispersed in a colloidal solution, and the values predict the colloidal stability; particles with zeta potential > ca. 30 mV are considered stable.[44] The isoelectric point, at which the AgNp charge is null, was obtained at a pH close to 3.8 (see Figure 1e). The zeta potential values at the synthesis pH of 9.4 were equal to –51 mV. This negative value is probably related to the negative charges of the citrate ions that surround the nanoparticles. Both the increase and decrease of the synthesis solution pH led to a reduction in the stability of the colloidal solution; however, the AgNp solution became in fact unstable only at pH values lower than 5.

In the TEM image shown in Figure 1f, the Ag nanoparticles present a spherical shape. With the help of the ImageJ software,[45] AgNp was counted from several such images, allowing the obtention of the particle size distribution; Figure 1g shows that the more frequent particle sizes are distributed between 1.5 and 6 nm, with a mean size of (4 ± 1) nm, which is an excellent result when compared to those in the literature. AgNp can be synthesized by physical, chemical, and biological methods, with sizes in the range 1-100 nm. Among the chemical methods, reduction with borohydride seems to be the most popular method because it provides a more precise control of the particle size.[24] Using this reducing agent, Bélteky *et al.*[46] and Wang *et al.*[47] obtained AgNp spheres of size ca. 10 nm. Agnihotri *et al.*[48] performed controlled syntheses of silver nanoparticles over the range of 5-100 nm. Corroborating these studies, Al-Marhaby and Seoudi[49] reported AgNp sizes of approximately 9, 11 and 14 nm.

The AgNp size and size distribution were also characterized by DLS analyses. The particle sizes were more frequent between 6 and 12 nm, with an average size of (9.00 ± 2.17) nm (see Figure 1h). These values are higher than the ones obtained by TEM, probably because the DLS technique assesses the hydrodynamic diameter of
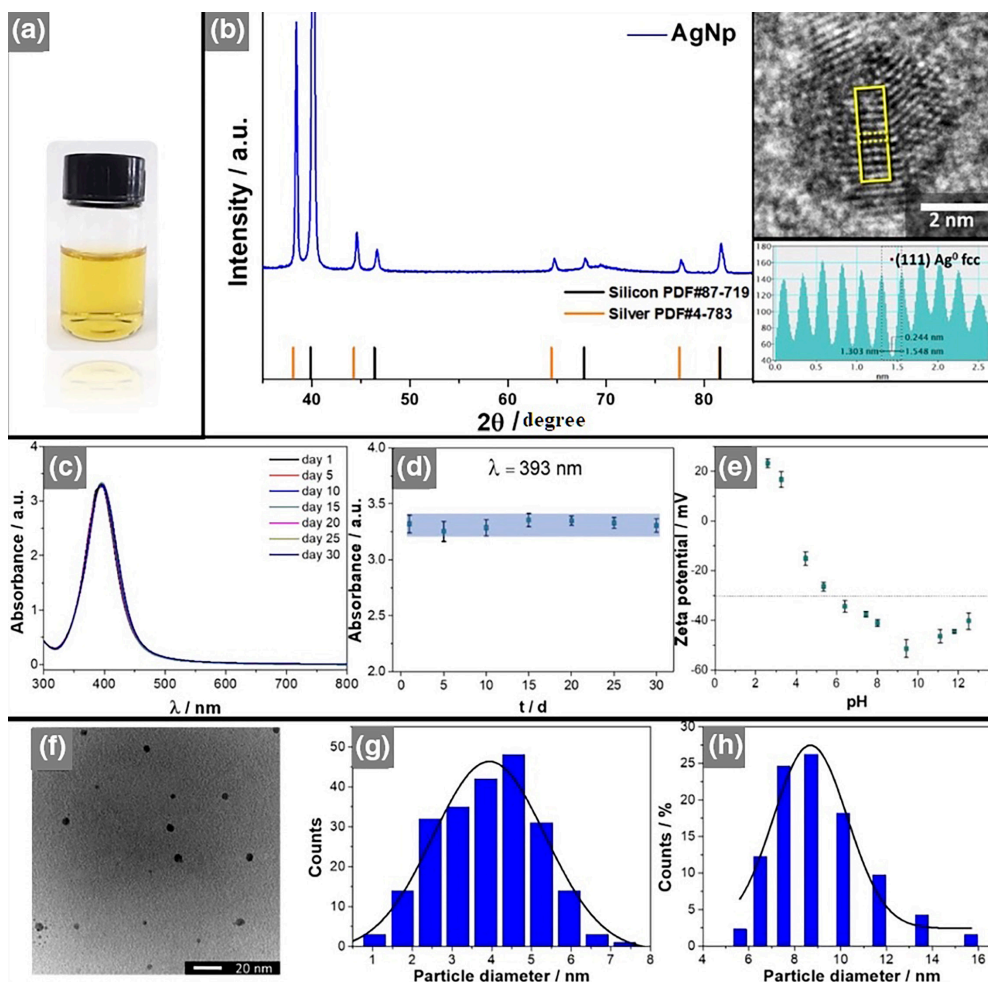
Figure 1. AgNp characterization: (a) solution visual aspect; (b) X-ray diffractogram, high-resolution TEM image and contrast profile (white-black) referring to the area highlighted in yellow; (c) AgNp solution (pH = 9.4) UV-Vis spectra acquired as a function of time (indicated in the (d) maximum absorbance (at λ = 393 nm) of the AgNp solution as a function of time); (e) zeta potential of the AgNp solution as a function of pH; (f) TEM micrograph; (g) and (h) particle diameter distribution obtained by TEM and DLS, respectively.

the particle, while the other refers to only the size of the particle itself.[28,50]

Characterization of the modified Ti/TiO$_2$/AgNp surface

A bioactive micro-porous TiO$_2$ coating containing Ca and P in the oxide layer obtained by MAO was described in a previous work.[10] As mentioned before, AgNp was deposited on the resulting TiO$_2$ porous surfaces. Figures 2a-2d show SEM micrographs of the anodized (An) TiO$_2$ surfaces after dripping on them different volumes of the AgNp solution: 3, 5, 10, and 15 mL. It is evident that the greater the dripped volume, the greater is the amount of deposited Ag. For the volumes 3, 5 and 10 mL, the deposited Ag presents a globular morphology and a uniform distribution on the TiO$_2$ surface. Furthermore, for the dripped volume 15 mL, a preferential deposition of AgNp around the pores can also be observed, as evidenced by the formation of agglomerates.

Regarding the antimicrobial tests, as can be seen in Figure 2e, all Ti/TiO$_2$/AgNp surfaces showed inhibition zones, indicating a positive response concerning the antimicrobial activity against the Gram-positive *Staphylococcus aureus* bacteria. The greater the dripped volume of the AgNp solution on the TiO$_2$ sample, the greater is the inhibition zone diameter, except for the 15 mL volume, for which a reduction was observed (see Figure 2f). This is most likely due to Ag agglomeration during the obtention of these samples, which may have led to a smaller surface area of this antimicrobial material. Thus, considering that Ag excess can be toxic to cells, it was decided to use the smallest dripping volume that showed antimicrobial activity, that is, 3 mL. From now on, this sample will be referred to as the 3mL sample.

Figure 3a shows the X-ray diffraction pattern of a 3mL Ti/TiO$_2$/AgNp sample. Several peaks for TiO$_2$ in the anatase phase could be identified. For AgNp, the spectrum exhibits a peak around 44.3° and another, of lower intensity, at

J. Braz. Chem. Soc. **2024**, *35*, 3, e-20230134

7 of 14
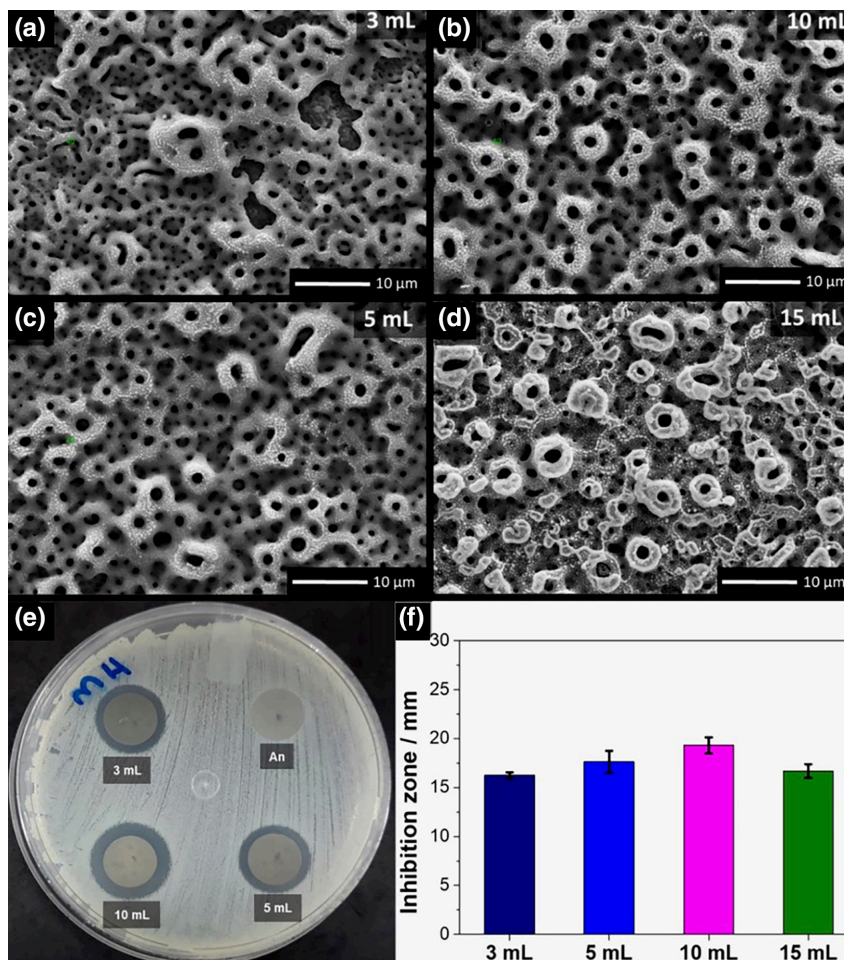
Figure 2. (a-d) SEM micrographs of the anodized Ti and Ag-deposited samples using AgNp solution volumes of 3, 5, 10, and 15 mL; (e) photograph of the inhibition zones, where An = anodized (negative control, Ti/TiO$_2$ sample); (f) comparison between the triplicate mean values of the inhibition zone diameters. *Statistical difference between groups, $p > 0.05$.
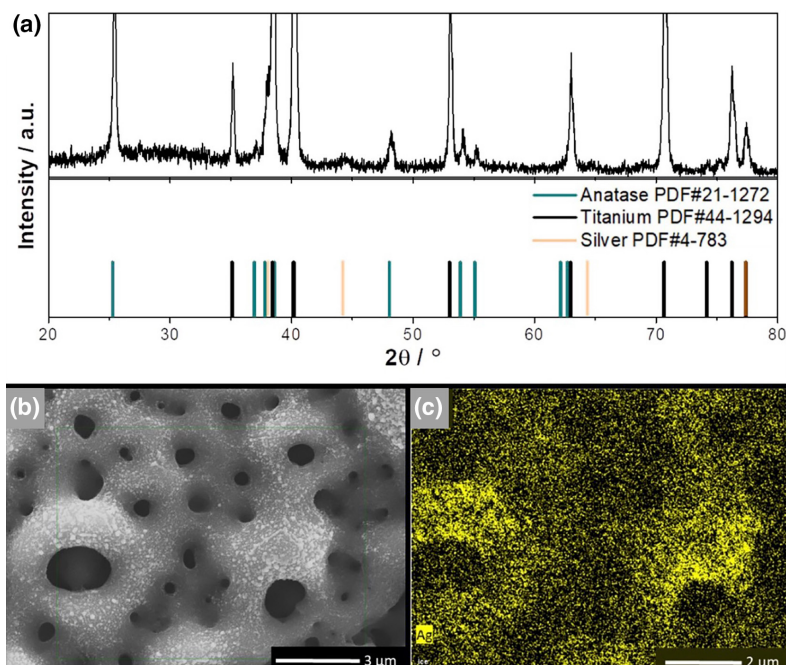
Figure 3. (a) XRD spectra, (b) SEM image, and (c) Ag EDS mapping for a 3mL Ti/TiO$_2$/AgNp sample.

64.4°, corresponding to the crystalline planes (200) and (220), respectively, as found in the crystallographic record JCPDS-PDF No.4-783 for metallic silver of cubic structure. Additionally, EDS measurements were performed, confirming the presence of Ag in the 3mL sample (data not provided). Finally, to evaluate the distribution of Ag on the TiO_2 surface, an EDS elemental mapping was performed (see Figure 3c), indicating both the presence and uniform distribution of silver on the surface.

Characterization of the modified Ti/TiO₂/PLA surface

The deposition time and PLA concentration were investigated to optimize the PLA polymer fiber coating procedure on the anodized Ti (An samples). All fibers obtained with PLA 10% (m/m) solutions exhibited the presence of beads, as evidenced in Figure 4a. On the other hand, the fibers obtained with the PLA 14% (m/m) solution were uniform and bead-free (see Figure 4b). According to Gu and Ren,[51] increasing the polymer solution concentration leads to the formation of more uniform fibers.

The electrospinning with PLA was carried out for 2, 3, 4, 5, 10 and 15 min (data not displayed) on the anodized Ti surfaces and, in general, a greater coverage of the sample was attained as the spinning time increased. Due to this, the 15 min spinning time was chosen to perform the coating process. Hereinafter, the 3mL samples coated with the polymer are referred to as 3mLPLA samples, whereas the PLA-coated An sample is referred to as the AnPLA sample.

The fiber diameter distribution was analyzed through the SEM micrograph of the 15 min polymeric coating shown in Figure 4c, with the help of the ImageJ software.[45] As can be inferred from the data in Figure 4d, the obtained fibers are ultrafine, most of them with diameters between 0.60 and 1.20 μm, with a mean value of 0.93 ± 0.26 μm.

Antimicrobial tests

The disk diffusion test was also performed after the Ti/TiO₂/AgNp samples were coated with the PLA polymer to verify whether the antimicrobial activity would be maintained. No formation of inhibition zone was found (see Figure 5B), probably because the PLA coating delays the Ag diffusion to the medium. It is worth mentioning that once the bacteria have already formed colonies on the agar, even if the antimicrobial agent diffuses and triggers bacterial death it will no longer result in the formation of an inhibition zone. This happens because, as the cellular debris remains, it is impossible to visually verify the death of the microorganisms. Another important factor is that due to the PLA hydrophobic character, the inoculum did not spread as efficiently as on the other surfaces.

As the disk diffusion test may not have been adequate to evaluate the antimicrobial activity in the PLA-coated samples, an adaptation of the Japanese standard JIS Z 2801[40] was used for a better evaluation. In this standard, the inoculum stays in direct contact with the sample surface and a polyethylene film is placed over it to promote a better
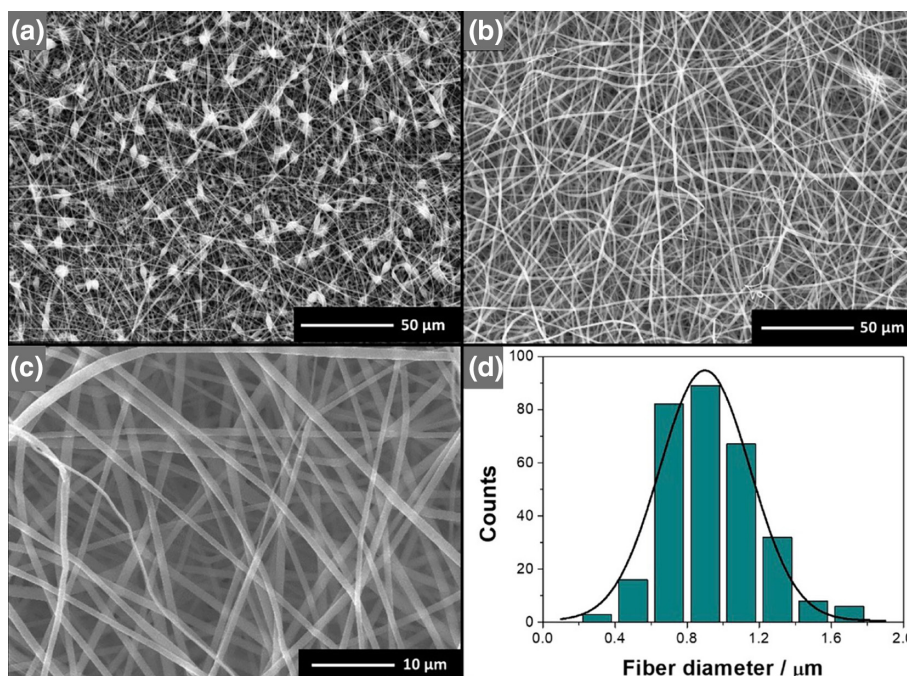
Figure 4. SEM images of the PLA coatings obtained on anodized Ti by electrospinning with the PLA 10% m/m solution for 10 min (a) or with the 14% m/m solution for 10 min (b) or 15 min (c). (d) Diameter distribution of the fibers displayed in (c).

J. Braz. Chem. Soc. **2024**, *35*, 3, e-20230134

9 of 14

spreading. Therefore, Ag diffusion to the suspension could be more efficient than that for the disk diffusion test. As described in the Experimental section, after incubation, a serial dilution of the suspension was performed and inoculated into PCA agar by the spread plate/pour plate method. Figure 5D illustrates the result of antimicrobial activity by the spread plate method of the An sample, which was used as a negative control. The formation of colonies up to the 10^{-2} dilution was noted. The pour plate method was not performed for the negative control.

No growth of CFU was observed in the case of the 3mL sample for both seeding methods: pour plate and spread plate. However, for the sample coated with PLA (see Figure 5D), CFU was formed but to a lesser extent than for the control. This result corroborates the hypothesis raised after reading the results of the disk diffusion tests. Most likely, PLA causes a delay in the silver diffusion; in addition, as PLA is a hydrophobic polymer, it was notable that even with the use of the polyethylene film on the inoculum, there was not a complete spread over the sample surface. This leads to a smaller contact area between the inoculum and the sample, which may also be generating the decrease of antimicrobial activity for these samples.

Quantitatively, the 3mL sample provided a CFU reduction greater than 4 orders of magnitude compared to the control (see Figure 5C), which corresponds to the death of practically all bacteria. Although the 3mLPLA sample did not cause a significant reduction in CFU as the uncoated one, it still showed a significant reduction, about 83%, compared to the An sample (see Table 2).

Table 2. CFU reduction of *S. aureus* according to the adapted JIS Z 2801 (2010) standard[40] for the An (control), 3mL, and 3mLPLA samples

	Control	3mL	3mLPLA
CFU reduction / %	0.0[a]	99.998[b]	83.165[c]
Standard deviation	0.0	0.000	27.073

[a,b,c]Statistical difference between the marked groups, $p > 0.05$. CFU: colony forming units.

Jia *et al.*,[27] investigating surfaces similar to the ones produced in this work, proposed that their antimicrobial activity is mainly related to three factors: (*i*) repulsion of bacteria by the silver ions released to the medium; (*ii*) death by contact between bacteria and the Ag surface; (*iii*) synergistic. Furthermore, they proposed that the existence of Ag inside the material pores makes these cavities a "death trap" for bacteria, because once inside it becomes impossible to free themselves alive. An aggravating factor for the bacteria is that their metabolism acidifies the medium, causing a faster silver dissolution and thus potentiating its antimicrobial activity.

According to Qing *et al.*,[52] AgNp exhibits two antibacterial mechanisms that are widely accepted: contact death and Ag ion-mediated death. Moreover, it is believed
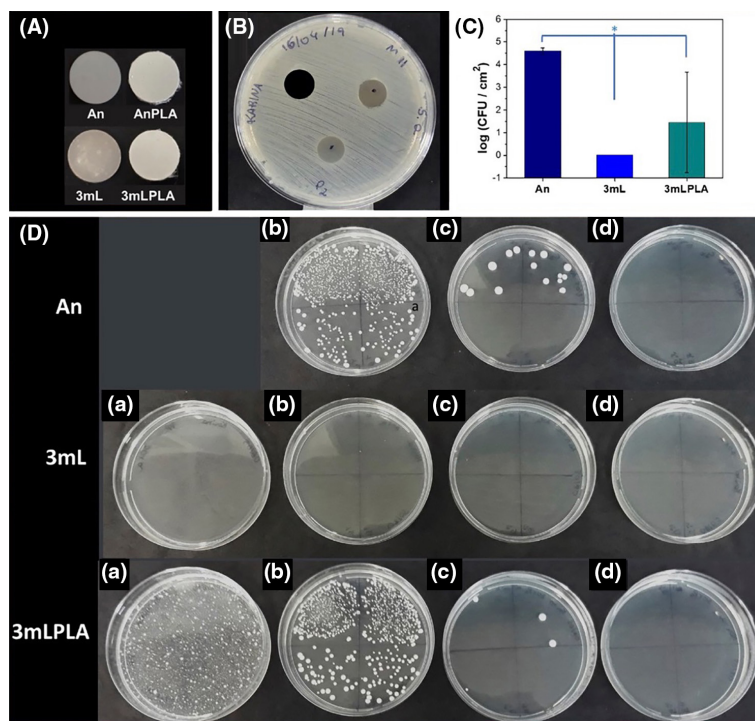
Figure 5. (A) Sample photographs, (B) disc diffusion test; (C) CFU counts of the *S. aureus* bacterium for samples: An, 3mL and 3mLPLA. *Statistical difference between the control group (An) and the others, $p > 0.05$. (D) (a) Pour plate method; and spread plate method in the dilutions: (b) upper quadrants 10^0 and lower quadrants 10^{-1}, (c) upper quadrants 10^{-2} and lower quadrants 10^{-3} and (d) upper quadrants 10^{-4} and lower quadrants 10^{-5}.

10 of 14

J. Braz. Chem. Soc. **2024**, *35*, 3, e-20230134

that there is a synergism between these mechanisms.[53] Thus, it is likely that the polymeric coating minimizes the antibacterial activity of Ag by inhibiting the contact death mechanism. Furthermore, the extremely superior response of the 3 mL sample is most likely related to this synergism.

Biocompatibility tests

The alamarBlue® test was performed to analyze cell viability on the produced surfaces. In this test, viable cells reduce the blue, non-fluorescent, resazurin compound to the reddish, fluorescent resorufin compound. Therefore, the test is directly correlated with the reduction of salt in the osteogenic medium and the density of live cells, indicative of cell growth and metabolic activity.[13,54]

The cell viability was evaluated for the An, AnPLA, 3mL, and 3mLPLA samples, but none of them showed cytotoxicity for pre-osteoblasts to the point of impairing cellular metabolism (see Figure 6a). Furthermore, there was no significant difference between groups ($p > 0.05$). Similar results were found in other *in vitro* or *in vivo* studies: the addition of AgNp did not lead to a different response than that of the control (Ti without Ag) and showed some alteration only in the initial periods.[27,28,55]

Next, the images obtained by direct fluorescence microscopy were analyzed to investigate cell morphology and spreading on the different Ti surfaces at 1, 3 and 7 days of culture. In this technique, the nucleus is stained in blue and the cytoplasm in green. As can be seen in Figure 6c, all samples allowed cell differentiation. The groups with polymeric coating stood out, as the pre-osteoblasts presented more evident cytoplasmic extensions, also called filopodia. According to Ren *et al.*,[56] more elongated morphologies (spindle-shaped cells), such as those for these samples, suggest greater metabolic activity. On the other hand, the An and the 3mL groups exhibited more rounded and ovoid cells, demonstrating a less advanced stage of development.

Although pictures of the An group suggest more advanced cell proliferation, this analysis cannot confirm it. In the PLA coating groups, the surfaces are more three-dimensional than in the groups without the polymer, making it difficult to compare the number of cells, since this greater three-dimensionality leads to a greater infiltration of the samples by the cells, which are not visualized in a bi-dimensional picture.

Finally, mineralized nodule formation was evaluated with the alizarin red test after 21 days of cell culture.
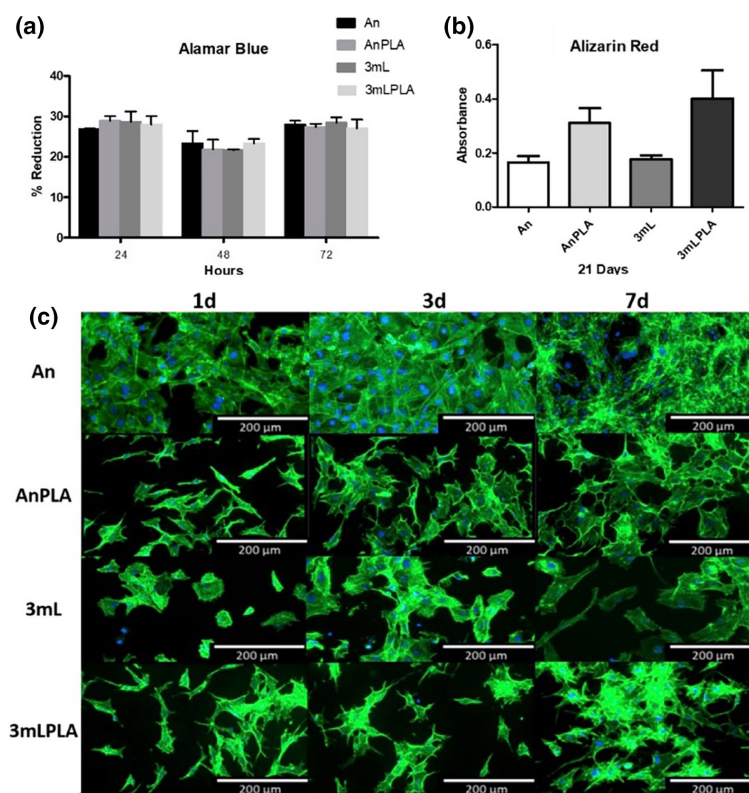
Figure 6. (a) Alamar Blue test within 24 and 72 h for the An, AnPLA, 3mL, and 3mLPLA samples (no significant difference was observed between groups, $p > 0.05$); (b) formation of extracellular mineralization nodules from the An, AnPLA, 3mL, and 3mLPLA samples after 21 days of cell culture (no significant difference was observed between groups, $p > 0.05$); (c) direct fluorescence micrographs of cells grown on the An, AnPLA, 3mL, and 3mLPLA samples at 1, 3 and 7 days of culture.

J. Braz. Chem. Soc. **2024**, *35*, 3, e-20230134

11 of 14

All groups showed nodules of extracellular matrix mineralization, which characterizes the presence of mature and active osteoblasts. After the dye solubilization, the absorbance reading of these solutions was performed. Corroborating with the fluorescence results (more stellate or stretched cells), the groups with polymeric coating tended to present more osteogenic mineralization processes, although without a significant difference between groups (see Figure 6b).

Silver-ion release

Figure 7 shows the daily release of Ag$^+$ from the 3mL and 3mLPLA samples in the PBS solution, at 37 °C, in the absence of light, in the first 15 days. The release profiles of these samples are similar. Initially, there is a greater release of Ag$^+$, which decreases with time. However, it is notable that the silver-ion release from the 3mLPLA sample was considerably lower in the first 10 days, indicating that the PLA coating effectively hampered the Ag$^+$ release to the medium. The risk of infection from dental implants is greatest in the first days after implantation. Thus, the release of silver should be greater during this period.[57] Therefore, according to the profiles exhibited for the 3mL and 3mLPLA samples, both samples are promising for combating implant-related infections.

Furthermore, the range of Ag threshold values for cell apoptosis is 0.78-1.56 µg mL^{-1}.[57,58] The 3mL sample showed the highest Ag release on the first day, equal to 0.36 µg mL^{-1}, well below this threshold. Therefore, the here-analyzed surfaces are not considered toxic. On the other hand, they are promising as antibacterial materials, since the minimum silver concentration for *S. aureus* inhibition is lower than 4 µg mL^{-1}.[59]

After the first 15 days of Ag$^+$ release, the PBS medium was collected and replaced. Then, the medium was changed only weekly, four times, to obtain an extended silver-ion release profile that allowed the greatest amount of deposited silver (see Figure 7b). In addition, on the last day of medium collection, the samples were dried at 60 °C for 24 h and submitted to an extraction process with concentrated nitric acid to dissolve and quantify all the remaining silver. Therefore, the total amount of silver from each sample could be obtained. As can be seen in Table 3, the silver-ion concentration released by the 3mL sample is higher than the one by the 3mLPLA sample, probably because some Ag was retained in the polymer bulk.

Table 3. Total silver-ion concentration released by the 3mL and 3mLPLA samples

Sample	[Ag$^+$] / (µg mL^{-1})	Standard deviation
3mL	3.8	0.2
3mLPLA	2.2	0.1

For the analysis of the silver-ion release by the samples without the PLA coating, the total silver amount was calculated for each sample as its amount accumulated over the periods, in addition to the amount removed by extraction after 43 days. However, as the PLA coating did not allow the total extraction of Ag from the coated surfaces, the average total amount of silver extracted from the 3mL sample was also used for the 3mLPLA sample. As can be seen in Figure 7b, on day 43 most of the deposited silver (89.1%) was released by the 3mL sample. This value was ca. 33% lower for the 3mLPLA sample, indicating that the PLA coating controls the release of silver to the medium.

According to Du *et al.*,[60] Ag nanoparticles with diameters from 12 to 38 nm showed antioxidant properties, exhibited antibiofilm activity and were biocompatible at Ag amounts up to 10 µg mL^{-1}, a value much higher than the maximum accumulated observed in this work (ca. 3.5 µg mL^{-1}).

Qin *et al.*[61] showed that AgNp immobilized on Ti surface has a lower cytotoxicity than when in suspension and, regardless of the Ag release, can reduce implant-associated periprosthetic infection. Hence, it is very interesting that a
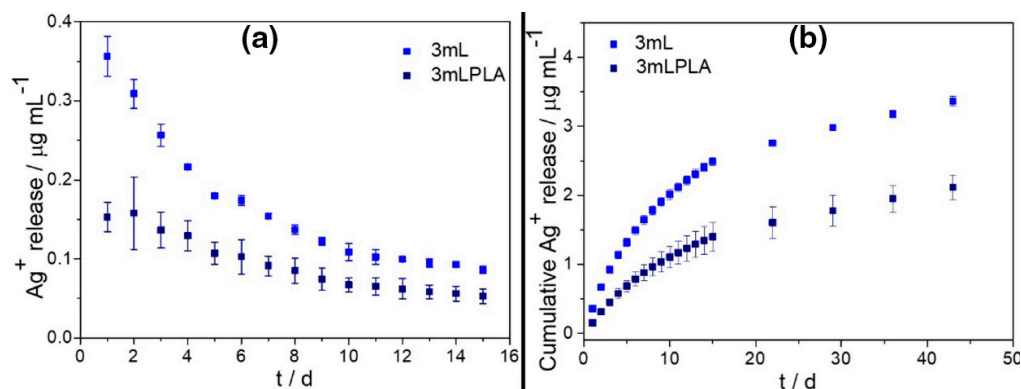
Figure 7. (a) Daily and (b) cumulative Ag$^+$ release, for the 3mL and 3mLPLA samples (indicated in the figures), quantified through ICP-OES.

silver amount stays on the titanium surface over time. The results obtained in this work for both the Ti/TiO$_2$/AgNp and Ti/TiO$_2$/AgNp/PLA samples are promising since the release of silver to the medium lasted for more than 40 days, a time long enough for implant osseointegration.

Conclusions

Biocompatible and antibacterial modified Ti surfaces were obtained with Ag nanoparticles (AgNp) and a polymeric coating of poly(latic acid) (PLA). The route employed to synthetize the silver nanoparticles allowed the obtention of ca. 4 nm spherical particles that were deposited homogeneously on the porous TiO$_2$ surfaces as indicated by the SEM micrographs and EDS mapping. Tests revealed that all AgNp-containing surfaces showed antimicrobial activity against *S. aureus*, with better results for the surfaces without the PLA polymeric coating. Furthermore, all surfaces presented good biocompatibility in tests with mouse MC3T3-E1 pre-osteoblasts, suggesting greater cell differentiation for the polymer-coated surfaces, probably due to the three-dimensional morphology of these surfaces. Finally, the PLA microfibers electrospun uniformly on the TiO$_2$/AgNp surfaces allowed a controlled silver-ion release in the PBS medium.

Acknowledgments

Author Contributions

All authors contributed to the formal analysis and to the manuscript writing-review and editing. S.R.B., R.C.R.-F. and N.B. were responsible for supervision, project administration and funding acquisition. K.M.Z. carried out the methodology, investigation, data curation and wrote the original draft.

References

1. Mas-Moruno, C.; Su, B.; Dalby, M. J.; *Adv. Healthcare Mater.* **2019**, *8*, 1801103. [Crossref]

2. Wei, Y.; Liu, Z.; Zhu, X.; Jiang, L.; Shi, W.; Wang, Y.; *Biomaterials* **2020**, *257*, 120237. [Crossref]

3. Hasan, J.; Bright, R.; Hayles, A.; Palms, D.; Zilm, P.; Barker, D.; Vasilev, K.; *ACS Biomater. Sci. Eng.* **2022**, *8*, 4697. [Crossref]

4. Saini, M.; Singh, Y.; Arora, P.; Arora, V.; Jain, K.; *World J. Clin. Cases* **2015**, *3*, 52. [Crossref]

5. Elias, C. N.; Fernandes, D. J.; Souza, F. M.; Monteiro, E. S.; Biasi, R. S.; *J. Mater. Res. Tech.* **2019**, *8*, 1060. [Crossref]

6. Shalabi, M. M.; Gortemaker, A.; Van't Hof, M. A.; Jansen, J. A.; Creugers, N. H.; *J. Dental Res.* **2006**, *85*, 496. [Crossref]

7. Civantos, A.; Martínez-Campos, E.; Ramos, V.; Elvira, C.; Gallardo, A.; Abarrategi, A.; *ACS Biomater. Sci. Eng.* **2017**, *3*, 1245. [Crossref]

8. Mi, G.; Shi, D.; Wang, M.; Webster, T. J.; *Adv. Healthcare Mater.* **2018**, *7*, e1800103. [Crossref]

9. Wang, Y.-R.; Yang N.-Y.; Sun, H.; Dong, W.; Deng, J.-P.; *J. Biomed. Mater. Res., Part B* **2023**, *111*, 846. [Crossref]

10. Zaniolo, K. M.; Biaggio, S. R.; Cirelli, J. A.; Cominotte, M. A.; Bocchi, N.; Rocha-Filho, R. C.; *Mater. Res. Express* **2022**, *9*, 025401. [Crossref]

11. Wang, Q.; Zhou, P.; Liu, S.; Attarilar, S.; Ma, R. L.-W.; Zhong, Y.; Wang, L.; *Nanomaterials* **2020**, *10*, 1244. [Crossref]

12. Lu, X.; Mohedano, M.; Blawert, C.; Matykina, E.; Arrabal, R.; Kainer, K. U.; Zheludkevich, M. L.; *Surf. Coat. Technol.* **2016**, *307*, 1165. [Crossref]

13. Soares, P.; Dias-Netipanyj, M. F.; Elifio-Esposito, S.; Leszczak, V.; Popat, K.; *J. Biomater. Appl.* **2018**, *33*, 410. [Crossref]

14. Singh, A.; Singh, B. P.; Wani, M. R.; Kumar, D.; Singh, J. K.; Singh, V.; *Bull. Mater. Sci.* **2013**, *36*, 931. [Crossref]

15. Raphel, J.; Holodniy, M.; Goodman, S. B.; Heilshorn, S. C.; *Biomaterials* **2016**, *84*, 301. [Crossref]

16. Gulati, K.; Ramakrishnan, S.; Aw, M. S.; Atkins, G. J.; Findlay, D. M.; Losic, D.; *Acta Biomater.* **2012**, *8*, 449. [Crossref]

17. De Giglio, E.; Cometa, S.; Ricci, M. A.; Cafagna, D.; Savino, A. M.; Sabbatini, L.; Orciani, M.; Ceci, E.; Novello, L.; Tantillo, G. M.; *Acta Biomater.* **2011**, *7*, 882. [Crossref]

18. Liu, Y.; Zheng, Z.; Zara, J. N.; Hsu, C.; Soofer, D. E.; Lee, K. S.; Siu, R. K.; Miller, L. S.; Zhang, X.; Carpenter, D.; Wang, C.; Ting, K.; Soo, C.; *Biomaterials* **2012**, *33*, 8745. [Crossref]

19. Kim, D.; Kwon, S. J.; Wu, X.; Sauve, J.; Lee, I.; Nam, J.; Kim, J.; Dordick, J. S.; *ACS Appl. Mater. Interfaces* **2018**, *10*, 13317. [Crossref]

20. Shi, D.; Mi, G.; Wang, M.; Webster, T. J.; *Biomaterials* **2019**, *198*, 228. [Crossref]

21. dos Santos, S. S.; de Couto, R. A. A.; da Silva, I. R.; Aouada, M. R. M.; Costantino, V. R. L.; da Costa, L. P.; Perotti, G. F.; *J. Braz. Chem. Soc.* **2023**, *34*, 705. [Crossref]

22. Oliveira, L. M. F.; da Silva, U. P.; Braga, J. P. V.; Teixeira, A. V. N. C.; Ribon, A. O. B.; Varejão, E. V. V.; Coelho, E. A. F.; de Freitas, C. S.; Teixeira, R. R.; Moreira, R. P. L.; *J. Braz. Chem. Soc.* **2023**, *34*, 527. [Crossref]

23. Vishwanath, R.; Negi, B.; *Curr. Res. Green Sustainable Chem.* **2021**, *4*, 100205. [Crossref]

J. Braz. Chem. Soc. **2024**, *35*, 3, e-20230134

13 of 14

24. Pryshchepa, O.; Pomastowski, P.; Buszewski, B.; *Adv. Colloid Interface. Sci.* **2020**, *284*, 102246. [Crossref]

25. Aydogan, D. T.; Muhaffel, F.; Kilic, M. M.; Acar, O. K.; Cempura, G.; Baydogan, M.; *Mater. Technol.* **2018**, *33*, 119. [Crossref]

26. López-Ortega, A.; Viteri, V. S.; Alves, S. A.; Mendoza, G.; Fuentes, E.; Mitran, V.; *Biomater. Adv.* **2022**, *138*, 212875. [Crossref]

27. Jia, Z.; Xiu, P.; Li, M.; Xu, X.; Shi, Y.; Cheng, Y.; *Biomaterials* **2016**, *75*, 203. [Crossref]

28. Li, Y.; Yang, C.; Yin, X.; Sun, Y.; Weng, J.; Zhou, J.; Feng, B.; *J. Mater. Chem. B* **2019**, *7*, 3546. [Crossref]

29. Liu, J.; Hurt, R. H.; *Environmental Sci. Technol.* **2010**, *44*, 2169. [Crossref]

30. Das, B.; Tripathy, S.; Adhikary, J.; Chattopadhyay, S.; Mandal, D.; Dash, S. K.; *J. Biol. Inorg. Chem.* **2017**, *22*, 893. [Crossref]

31. Damle, A.; Sundaresan, R.; Rajwade, J. M.; Srivastava, P.; Naik, A.; *Biomater. Adv.* **2022**, *141*, 213099. [Crossref]

32. Zhang, L.; Ning, C.; Zhou, T.; Liu, X.; Yeung, K. W.; Zhang, T.; *ACS Appl. Mater. Interfaces* **2014**, *6*, 17323. [Crossref]

33. Nofar, M.; Sacligil, D.; Carreau, P. J.; Kamal, M. R.; Heuzey, M. C.; *Int. J. Biol. Macromol.* **2019**, *125*, 307. [Crossref]

34. Kravanja, K. A.; Finšgar, M.; *Mater. Des.* **2022**, *217*, 110653. [Crossref]

35. Smith, J. R.; Lamprou, D. A.; *Trans. IMF* **2014**, *92*, 9. [Crossref]

36. Haider, A.; Haider, S.; Kang, I.-K.; *Arabian J. Chem.* **2018**, *11*, 1165. [Crossref]

37. Mohiti-Asli, M.; Pourdeyhimi, B.; Loboa, E. G.; *Acta Biomater.* **2014**, *10*, 2096. [Crossref]

38. Munteanu, B. S.; Aytac, Z.; Pricope, G. M.; Uyar, T.; Vasile, C.; *J. Nanopart. Res.* **2014**, *16*, 2643. [Crossref]

39. Chen, W.; Chen, S.; Morsi, Y.; El-Hamshary, H.; El-Newhy, M.; Fan, C.; Mo, X.; *ACS Appl. Mater. Interfaces* **2016**, *8*, 24415. [Crossref]

40. Japanese Industrial Standard, JIS Z 2801:2010: *Antibacterial Products-Test for Antibacterial Activity and Efficacy*, 2010.

41. Clinical and Laboratory Standards Institute (CSLI); CLSI document M100-S15: *Performance Standards for Antimicrobial Susceptibility Testing; Fifteenth Informational Supplement*; Clinical and Laboratory Standards Institute, Wayne, PA, USA, 2005.

42. Pyatenko, A.; Yamaguchi, M.; Suzuki, M.; *J. Phys. Chem. C* **2007**, *111*, 7910. [Crossref]

43. Singh, R.; Shedbalkar, U. U.; Wadhwani, S. A.; Chopade, B. A.; *Appl. Microbiol. Biotechnol.* **2015**, *99*, 4579. [Crossref]

44. Leite, E. R.; Ribeiro, C.; *Crystallization and Growth of Colloidal Nanocrystals*; Springer New York, USA, 2012. [Crossref]

45. Schneider, C. A.; Rasband, W. S.; Eliceiri, K. W.; *Nat. Methods* **2012**, *9*, 671. [Crossref]

46. Bélteky, P.; Rónavári, A.; Igaz, N.; Szerencsés, B.; Tóth, I. Y.; Pfeiffer, I.; Kiricsi, M.; Kónya, Z.; *Int. J. Nanomedicine* **2019**, *14*, 667. [Crossref]

47. Wang, J.; Zhao, J.; Ma, G.; *Nano-Struct. Nano-Objects* **2019**, *19*, 100349. [Crossref]

48. Agnihotri, S.; Mukherji, S.; Mukherji, S.; *RSC Adv.* **2014**, *4*, 3974. [Crossref]

49. Al-Marhaby, F. A.; Seoudi, R.; *World J. Nanosci. Eng.* **2016**, *6*, 29. [Crossref]

50. Patil, R. B.; Chougale, A. D.; *Mater. Today: Proc.* **2021**, *47*, 5520. [Crossref]

51. Gu, S.-Y.; Ren, J.; *Macromol. Mater. Eng.* **2005**, *290*, 1097. [Crossref]

52. Qing, Y.; Cheng, L.; Li, R.; Liu, G.; Zhang, Y.; Tang, X.; Wang, J.; Liu, H.; Qin, Y.; *Int. J. Nanomedicine* **2018**, *13*, 3311. [Crossref]

53. Siritongsuk, P.; Hongsing, N.; Thammawithan, S.; Daduang, S.; Klaynongsruang, S.; Tuanyok, A.; Patramanon, R.; *PLoS One* **2016**, *11*, e0168098. [Crossref]

54. Al-Nasiry, S.; Geusens, N.; Hanssens, M.; Luyten, C.; Pijnenborg, R.; *Hum. Reprod.* **2007**, *22*, 1304. [Crossref]

55. Wang, J.; Li, J.; Guo, G.; Wang, Q.; Tang, J.; Zhao, Y.; *Sci. Rep.* **2016**, *6*, 32699. [Crossref]

56. Ren, L.; Pan, S.; Li, H.; Li, Y.; He, L.; Zhang, S.; *Sci. Rep.* **2018**, *8*, 15143. [Crossref]

57. Wan, Y.; Wang, G.; Ren, B.; Liu, Z.; Ge, P.; *Nanomanuf. Metrol.* **2018**, *1*, 252. [Crossref]

58. Marambio-Jones, C.; Hoek, E. M. V.; *J. Nanopart. Res.* **2010**, *12*, 1531. [Crossref]

59. Kim, J. S.; Kuk, E.; Yu, K. N.; Kim, J. H.; Park, S. J.; Lee, H. J.; Kim, S. H.; Park, Y. K.; Park, Y. H.; Hwang, C.-Y.; Kim, Y.-K.; Lee, Y.-S.; Jeong, D.-H.; Cho, M.-H.; *Nanomedicine* **2007**, *3*, 95. [Crossref]

60. Du, J.; Singh, H.; Yi, T. H.; *Bioprocess Biosyst. Eng.* **2016**, *39*, 1923. [Crossref]

61. Qin, H.; Cao, H.; Zhao, Y.; Zhu, C.; Cheng, T.; Wang, Q.; Peng, X.; Cheng, M.; Wang, J.; Jin, G.; Jiang, Y.; Zhang, X.; Liu, X.; Chu, P. K.; *Biomaterials* **2014**, *35*, 9114. [Crossref]

14 of 14

J. Braz. Chem. Soc. **2024**, *35*, 3, e-20230134